Urban scale risk assessment including SSI and site amplification

Chiara Amendola[1*] and Dimitris Pitilakis[1†]

[1*]Department of Civil Engineering, Aristotle University of Thessaloniki, Street, City, 54621, Greece, Country.

*Corresponding author(s). E-mail(s): chiaamen@civil.auth.gr;
Contributing authors: dpitilakis@civil.auth.gr;
[†]These authors contributed equally to this work.

Abstract

Large-scale risk analysis is typically performed considering existing fragility curves, calculated in most cases without adequately accounting for local site amplification (SA) and soil-structure interaction (SSI) effects. Nevertheless, foundation flexibility and local site effects may lead to a substantial margin of fragility or loss estimates, especially for structures resting on soft soil. Including these effects on the city-scale vulnerability analysis is challenging due to the entailed complexity of defining the whole interacting urban system. We propose a novel framework for the fragility assessment of structures considering the influence of SSI and local site amplification effects, suitable for large-scale applications. The applicability of the proposed approach is based on globally available data regarding the soil, the foundation, and the building portfolio. Site amplification is considered directly in the resulting fragility curves using site response analyses. An improved taxonomy is adopted to make the approach implementable in the OpenQuake software, introducing $\boldsymbol{V_{S,30}}$ as a proxy for the site and SSI effects. Finally, following the performance-based earthquake engineering framework, the outcomes of the methodological framework are adopted to estimate the nominal probability of failure for selected building classes belonging to the majority of structural types of the city of Thessaloniki, Northern Greece. The main findings demonstrate that the conventional way of calculating fragility curves may lead to an incorrect seismic risk evaluation, especially in soft soil formations.

Keywords: soil-foundation-structure-interaction, site-effects, fragility curves, city-scale risk analysis

1 Introduction

There has been a substantial increase in interest among researchers in seismic risk, which is essential in selecting and designing the most appropriate short- and long-term earthquake mitigation and after-emergency management. The corresponding accuracy depends on the many input parameters defining the risk model. Evaluating fragility curves, which represent the probability of exceedance of a predefined performance level for a given intensity measure (IM), is one inherent challenging task in the risk model assessment.

In a large-scale risk application, to reduce the computational effort, the risk analysis is performed by applying existing fragility functions, like the ones created in the framework of the Global Earthquake Model (GEM) initiative (Yepes-Estrada et al, 2016). The analytical fragility curves derived for large-scale analyses may have been estimated using records (generally a sizeable broad set) that do not correctly account for the variation in frequency and amplitude contents; the latter is imposed by local geotechnical and topographic conditions. Moreover, in large-scale applications, the complexity related to the characterization of the soil-foundation system, along with the common belief in the beneficial effects of soil-structure interaction (SSI), led to the development and application over the years of fragility functions following the fixed-base restrain hypothesis ((Riga et al, 2017; De Risi et al, 2019; Smerzini and Pitilakis, 2018; Riga et al, 2021) to mention few). Notwithstanding this, a series of research attempts recognized the modification of the fragility of structures founded on soft soil compared to the typical fixed-base assumption.

Incorporating such effects in the analytical computation of fragility functions has been accomplished by employing the different simplified approaches, based on the uncoupled 'substructure method,' refined complete SSI models based on the 'direct method,' or 'hybrid methods' based on domain reduction methods (NIST, 2012). Different results are obtained depending on the modeling approach adopted.

While site amplification (SA) is inherently taken into account when adopting the direct approach, the substructure method may be suitable for understanding the relevant contribution of SSI and SA to the modification of the dynamic response and thus of the fragility compared to the fixed-base assumption. Site amplification is generally shown to have a negative impact, while SSI may play a beneficial role in the resulting fragility curves enhanced by soil hysteresis (Brunelli et al, 2022).

Some literature efforts (Tomeo et al, 2018; Karapetrou et al, 2015) compared fragility curves obtained by employing the decoupled approach for fixed-base structures subjected to free-field motions and the results from the direct method. For the high-rise building designed with low seismic code provisions, Karapetrou et al (2015) found that SSI may lead to an increase in the overall fragility with respect to the fixed-base model subjected to SA, only when soil nonlinearity is considered. At the same time, no essential differences are observed when the soil profile is assumed linear elastic.

The assumption on the soil and, most notably, the soil-foundation behavior is found in all the studies to play a fundamental role in the resulting fragilities making even more cumbersome their employment in a generic risk framework. When considering soil nonlinearity, Saez et al (2011) observed an increase in the overall dissipation capacity

with respect to the pure linear SSI due to the hysteretic dissipation during earthquake loading. On the other hand, ignoring the nonlinear foundation effects (such as gapping, sliding, and uplift) may lead to an unconservative prediction of the structural demand and, consequently, a less fragile response (Figini et al, 2012; Rajeev and Tesfamariam, 2012). It is also worth mentioning that some of these studies (e.g. Karapetrou et al (2015); Karafagka et al (2021)) investigated the role of combined effects (e.g. aging or liquefaction) making the results strongly case-dependent. Even though the results of such studies provided the scientific community with valuable knowledge for site-specific vulnerability assessment, only recently some research efforts (Petridis and Pitilakis, 2020, 2021; Cavalieri et al, 2020), have paved the way toward an integrated large-scale procedure providing, for example, secondary factors to shift the existing fragility functions to include nonlinear soil and SSI effects (Petridis and Pitilakis, 2020, 2021).

Despite this last effort and the previous investigations, not all possible superstructure-foundation-soil scenarios have been considered so far, making questionable the collection of a database and its implementation in a uniform approach as required, for example, from a city-scale or regional level application.

To this aim, the present study intends to start filling the existing gap by developing and proposing a systematic methodology for estimating fragility curves of different classes of buildings considering SSI and local SA effects. We propose a novel framework for the fragility assessment of structures considering the influence of SSI and local site amplification effects, suitable for large-scale applications. The proposed method applies to many soil-foundation systems encountered in an urban environment and is designed explicitly for urban-scale risk assessment. To demonstrate its potential, we use the proposed approach to calculate the failure rates of the buildings in the city of Thessaloniki, in northern Greece.

2 Proposed method

This section aims to propose and quantify an analytical methodology to assess the fragility functions of different building classes founded on shallow or embedded foundations considering SSI and local SA effects. All the analyses are conceived to be implemented in the open-source OpenSees software (Mazzoni et al, 2006). However, the proposed fragility assessment scheme is easily applicable using different software. Figure 1 summarizes the whole methodological framework, whereas each step is described below:

- **Input**:
  - Our procedure starts with the definition of the input parameters. An extensive set of input ground motions is selected to formally consider the randomness of ground motions (Jalayer et al, 2017). We choose input motions recorded on outcropping bedrock or very firm soil (i.e., with $V_{S,30}$ greater than 700 m/s) since SA is directly simulated in the following step.

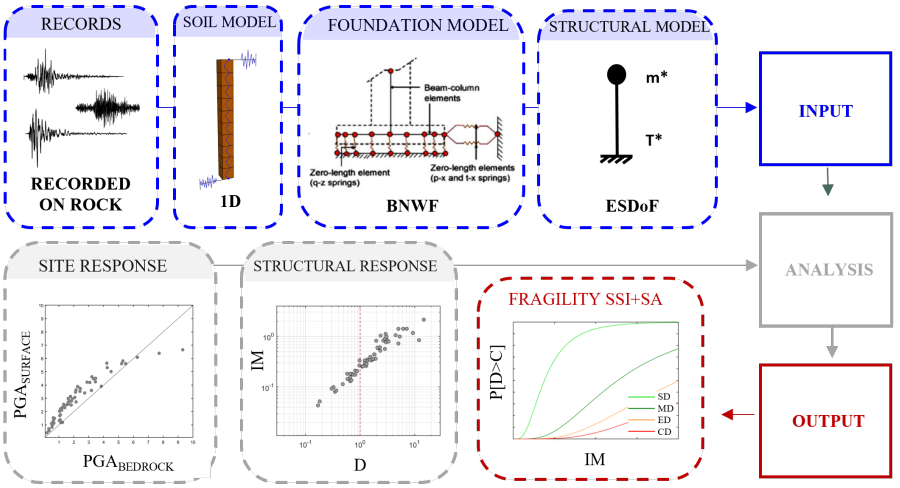

Fig. 1. Flow chart of the proposed methodology for the fragility assessment of structures considering SSI and SA at an urban scale

- The soil profile can be simulated in any software able to perform 1D (or 2D/3D) site response analyses. We use OpenSees to run the 1D analyses, using appropriate material models to simulate sandy or clayey soil profiles.
- To reduce the computational effort inherently entailed in large-scale applications, the structure is modeled as an equivalent single degree of freedom (ESDoF) system (D'Ayala et al, 2014).
- This ESDoF is placed on nonlinear horizontal and vertical springs and dashpots, simulating the compliance of the foundation subsoil using the Beam-on-Nonlinear-Winkler-Foundation (BNWF) concept (Harden et al, 2005).

• **Analysis**:

- This study presents effective probabilistic procedures for consideration of SA effects directly in the fragility curves rather than in the hazard. This approach provides more precise (i.e., with a minor degree of uncertainty) estimates of local site effects than when using amplification factors and/or functions for generic soil conditions. Since the uncertainties in the soil parameters play a secondary role compared to record-to-record variability (Bazzurro and Cornell, 2004; Rajeev and Tesfamariam, 2012), SA is quantified by running 1D wave propagation analyses by applying the selected earthquake records at the base of deterministically defined soil columns. The calculated free-field motion (FFM) inherently includes nonlinear site amplification effects.
- The free-field motions are selected as input at the base of the flexible-base ESDoF models to run all the dynamic cloud analyses (CA) (Jalayer et al, 2017). The FFM is directly applied as input for the dynamic calculations for structures resting on surface foundations. In contrast, for embedded foundations, the free-field motion

is further modified to consider the kinematic interaction before being applied at the base of the superstructure.

- **Output**:
  - An improved fragility model, notably the Modified Cloud analysis (MCA) (Jalayer et al, 2017), is adopted herein to compute fragility functions that formally consider the collapse-inducing records.
  - The statistical treatment of the results allows calculating the probability of exceeding four different limit states (slight, moderate, extensive, and complete damage state Martins and Silva (2020)). This framework provides the user with fragility functions accounting for SA and SSI.

One of the novelties of the proposed approach is to provide fragility functions classified according to the averaged shear-wave velocity in the top 30 m ($V_{S,30}$), and a foundation feature such as the slenderness ratio, H/B. $V_{S,30}$ and H/B are conceived in this work as proxies for the SA and SSI effects. As shown in the following, the advantage of the proposed method is the possibility of linking the so-modified taxonomy with actual soil conditions and foundation geometrical parameters, leading to a risk assessment framework in which SSI and SA are directly considered in the fragility analysis.

2.1 General criteria for the selection of the input data

his section provides guidelines for selecting input parameters from globally available databases. These criteria make the proposed framework easily applicable for risk assessment in different cities.

2.1.1 Earthquake record

Following the CA approach, we suggest selecting a large set of unscaled actual ground motions mostly recorded on outcrop rock to perform all the dynamic analyses (Jalayer et al, 2017). The reason behind this selection criterion is twofold; it allows considering a unique set of records for all the spatially distributed building portfolios. At the same time, this approach reduces uncertainties when investigating the site amplification effects compared to the more simplified soil class-compatible records selection.

2.1.2 Soil profile

To consider local site amplification effects and determine the soil's prominent features in the SSI modeling is necessary to define representative soil profiles. Following the city scale approach, these profiles should be based on detailed microzonation studies (if available). As an alternative, to fully cover the spatial variability of SA, a sufficient number of simplified soil profiles can be defined, varying the mean shear wave velocity to 30 m depth, $V_{S,30}$ to cover all the soil classes according to the specific country-regulation (e.g., CEN 2005 for Europe). On such a basis, the results of the analyses and thus the fragility functions will be dependent on $V_{S,30}$. The latter is critical in

implementing the proposed methodology, making the resulting fragility functions site-consistent. The updated taxonomy makes the proposed fragility functions accounting for SSI and SA implementable in the OpenQuake software (Pagani et al, 2014).

Among various site amplification proxies (Derras et al, 2017), we select $V_{S,30}$ to represent soil conditions since different approaches are currently available in the literature to compute $V_{S,30}$ maps from globally available data. The $V_{S,30}$-slope correlations proposed by (Wald and Allen, 2007) are well-established and already used for large-scale (and not local or site-specific) studies. These correlations concern using the topographic slope from digital elevation models (DEM) obtained from remote sensing (satellite imaging). The $V_{S,30}$ map estimates are also freely available on the USGS website (USG, USGS) for the whole world. Several studies have also attempted to correlate $V_{S,30}$ with geological units (e.g., Forte et al 2017), which are again available via geological maps at various scales for the entire globe via the One Geology portal (ONE, ONEGEO).

2.1.3 Foundation

Here, we account for SSI effects using the Beam-on-Nonlinear-Winkler-Foundation (BNWF) concept (Harden et al, 2005; Raychowdhury and Hutchinson, 2008). The BNWF element is modeled in Opensees by investigating the non-dimensional parameters influencing the seismic response of the soil-structure system to earthquake ground motion. The interaction parameters can be presented and determined by basic as follow (Veletsos and Meek, 1974):

1. the slenderness ratio of the building, (H/B), where B is the characteristic foundation half-length and H the structural height or effective height. This parameter can be retrieved from the building footprint area as available in the OpenStreetMap. The whole foundation system is reduced to an equivalent rectangular surface foundation defined as a function of the footprint area. The structural height H can be retrieved from the same open data source or the number of stories known from the building asset.
2. The structure-to-soil mass ratio index, $\delta = m/(H\rho\pi r^2)$ where m is the effective structural mass and ρ expresses the soil mass per unit volume. The practical range of structure-to-soil mass ratio does not vary enormously for conventional building types. Stewart et al (1999) suggest delta values between 0.1-0.2 while, more directly, Veletsos and Meek (1974) recommended delta equals 0.15. The definition of the latter parameter is of significant importance in the proposed approach since it allows for the description of the structural mass.
3. The soil-to-structure relative stiffness ratio, $\sigma = V_S/(fH)$, where f is the fundamental frequency of the fixed-base structure, which can be computed as a function of the structural height, H. Despite being the most effective index influencing the response of SSI systems, having already parametrized the SSI system as a function of δ, H/B and $V_{S,30}$, its definition is no longer necessary. Classification as a function of σ could automatically follow.

2.1.4 Structure

To make the proposed approach computationally efficient, buildings are classified by combining a few attributes such as lateral force resisting mechanism, height, and seismic design code level. This classification is also known as taxonomy (e.g., GEM taxonomy Brzev et al (2013)). To further reduce the computational effort (as implicitly demanded from seismic fragility assessment of building portfolios,) each building class is modeled following the equivalent single degree of freedom (ESDoF) systems approximation for the superstructure (D'Ayala et al 2014). Among the benefits, such an approach requires a limited number of parameters to be defined that can be determined from globally available data. Capacity curves for the characterization of the hysteretic low are available in the literature for a comprehensive set of building classes. For Europe, they are available in the GitHub repository by Martins and Silva (2020).

Once its parameters are defined, the ESDoF system can be easily implementable in OpenSees through a 'zero-length' or the 'twoNodeLink' element object. In SSI applications, while the former needs to be implemented with a rigid beam, the latter element can be preferred given its twofold nature (it can have zero or non-zero length). The 'twoNodeLink' with a non-zero length set equal to the effective structural height, H can be employed to consider the rocking-induced structural displacement. The element's implementation is then finalized by assigning different hysteretic relationships selected from the OpenSees material library depending on the structural type at hand. Given the availability of the OpenSees library, it is possible to consider the potential presence of strength and/or cyclic stiffness degradation in the hysteresis most relevant to the building class under consideration. Despite its simplicity, this modeling approach has been successfully adopted by different authors and thus proved to provide a pretty good representation of the dynamic response of actual structures subjected to seismic loading (Suzuki and Iervolino 2019).

3 Application

The objective of this section is twofold. First, we present a novel framework for the fragility assessment of structures considering the influence of SSI and local site amplification effects, suitable for large-scale applications. For this purpose, we selected as a case study the site of Thessaloniki, in northern Greece, which belongs to one of the most seismo-tectonically active zones in Europe. The decision also stems from the fact that there is an available plethora of data regarding the local geology and the exposed building portfolio for Thessaloniki.

As a second objective, we will show how especially in soft soil formations, the conventional way of calculating fragility curves for large-scale applications, i.e., fixed-base structures subjected to free-field motion, may lead to an incorrect evaluation of the seismic risk discussed in the following in terms of failure rates.

3.1 Input

3.1.1 Earthquake record selection

Within this application, records were selected from the ground motion database of the Pacific Earthquake Engineering Research center (NGA, NGAWEST) and the European (ISE, ISESD) and the Italian ITACA record (ITA, ITACA) databases. In detail, record selection was carried out following the general recommendation suggested in Jalayer et al 2017. Ground motion selection should be carried out, covering a vast range of intensity measure values.

Different intensity measures (IM) are selected in this study for the fragility computation. The IM that we chose is the pseudo-spectral acceleration at periods close to the fundamental period of the structure, $Sa(T)$, and the average spectral acceleration, $AvgSa$. The latter is of particular interest in SSI studies since it allows the comparison between fragility functions developed for different compliant systems and the reference curves considering the fixed-base assumption.

Following the same state-of-the-art approach, records should be selected respecting the focal mechanisms and soil type. The latter was the key recommendation guiding the whole record selection. Only records recorded on rock should be considered since SA is numerically implemented within the proposed method. No explicit consideration of the type of faulting was carried out because of the limited number of records available for stations on rock/stiff soil. Also, the selected records could not lead the structure to pass the onset of the near-collapse capacity threshold for some structural typologies. Some records were scaled up to a factor of 2 to avoid the unrealistic, undesired modifications of scaled signals. The selected unscaled records are reported in the Appendix A1 in the Electronic Supplements of this article.

All the chosen IM are computed for the set of input records (i.e., recorded on rock/very stiff soil) referred to in the following as PGA_R, $Sa(T)_R$, $AvgSa_R$ respectively.

3.1.2 Soil profile modeling

For the site response analysis and to define the soil input parameters for the BNWF model, seven different representative clayey soil profiles were modeled in OpenSees. The same approach can be easily applied for a sandy soil profile; nevertheless, previous works (Pitilakis and Petridis, 2020) on the topic recognized no critical differences in the final fragility curves. The selected soil profiles were conceived considering different average propagation velocities of the shear waves within the first 30m of soil depth, $V_{S,30}$ (i.e., ranging from 150 to 450 m/s) thus of soil types B, C and D according to the EC8 soil classification (CEN, 2005).

As reported in Figure 2 the adopted shear stiffness profile varies continuously with depth. A simplified distribution is considered in this study to describe the distribution of the soil shear stiffness, $V_S(z)$ with depth as follows:

$$V_S(z) = V_{S,z=30}\left(\left(\frac{V_{S,z=0}}{V_{S,z=30}}\right)^{\frac{1}{a}} + \frac{z}{30}\cdot\left(1-\left(\frac{V_{S,z=0}}{V_{S,z=30}}\right)^{\frac{1}{a}}\right)\right)^{a} \quad (1)$$

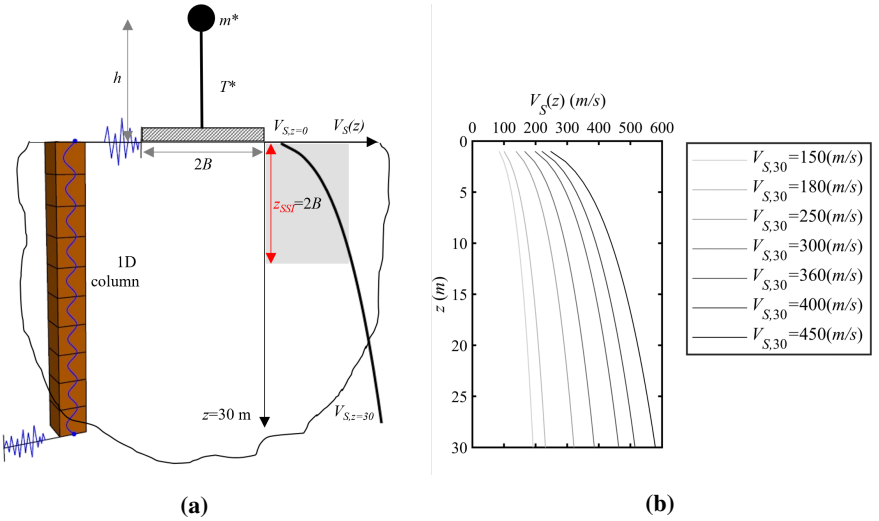

Fig. 2. (a) schematic view of the uncoupled SSI model comprising the structure foundation system and 1D soil column characterized by (b) the shear wave profiles of the seven different virtual soil profiles considered for the analysis ranging from very soft soil (light grey curves) to medium-stiff soil (dark grey curves).

Table 1. Main soil parameters selected to characterize the soil profile

Soil parameters							
$V_{S,30}$ (m/s)	150	180	250	300	360	400	450
Soil class	D	D/C	C	C	C/B	B	B
Type of soil	clay						
$cu(kPa)$	28	33	58	75	85	110	150
$\gamma(kN/m^3)$	15	17	18	19	20	20	21

where z stands for the depth measured from the soil surface, while $V_{S,z=0}$ and $V_{S,z=30}$ are the soil shear modulus at the ground surface and the depth of 30 meters, respectively. The $V_{S,z=0}$ and $V_{S,z=30}$ are selected to ensure a $V_{S,30}$ equal to the values reported in Table 1. The a coefficient was selected equal to 0.25.

As shown in Figure 2a the numerical model for the site response analysis is performed for a single column of soil deposit 30 meters deep and modeled by 'Quad' elements in OpenSees. The site response analysis is implemented in OpenSees using total stress analysis. The nonlinear behavior of the soil is modeled by assigning a nonlinear material to quad elements "nDMaterial PressureIndependMultiYield" (nonlinear constitutive law based on Von Mises criterion for clays). Table 1 summarizes the physical and mechanical properties assigned to the soil layers.

All the values reported in Table 1 have been selected from literature studies aimed at assessing the soil classification (e.g., Pitilakis et al 2019; Tropeano et al 2018). Such studies are based on a comprehensive analysis of a worldwide database of strong ground motions recorded on deeply characterized sites up to the bedrock. The energy dissipation in the soil is introduced through the Rayleigh damping formulation.

3.1.3 Foundation modeling

Nonlinear soil-foundation interaction through the BNWF model is automatically implemented in the OpenSees software through the 'shallow foundation generator' command (Raychowdhury and Hutchinson, 2008). It consists of elastic beam-column elements that capture the structural footing behavior with independent 'zero-length' soil elements that model the soil-footing behavior. The stiffness used to calibrate the zero-length elements should consider the effect of soil inhomogeneity (Vratsikidis and Pitilakis, 2019; Amendola et al, 2021).

Literature studies (Stewart et al, 2003; NIST, 2012) suggest to approximate soil inhomogeneity with an equivalent halfspace with representative values of V_S averaged over depths equal to 0.75 $r_{\theta x}$ and 0.75 r_x, where $r_{\theta x}$ and 0.75 r_x are the rocking and swaying equivalent radii. Accordingly, a unique value is selected as a function of a V_S mobilized considering an interaction volume equal to the total foundation length (grey shadowed zone in Figure 2a).

An equivalent radiation damping is calculated from the impedance functions following the procedure described in Amendola and Pitilakis (2022). Such a simplified approach allows considering the frequency dependence of the dissipation capacity of the foundation subjected to ground shaking, compared to the simplified assumption of fixed radiation damping.

To cover a wider variety of structures, various structural details/masses and aspect ratios are selected for each structural type or building class. The foundation parameters are defined from data gathered through a literature review of previous studies on SSI available for the case study of Thessaloniki, northern Greece (Pitilakis et al, 2014; Karapetrou et al, 2015; Petridis and Pitilakis, 2020, 2021; Karafagka et al, 2021). These studies mainly refer to moment frame (LFM), or frame plus shear wall (LDUAL) reinforced concrete (RC) buildings. Table 2 summarizes all the retrieved information, mainly the slenderness ratio, H/B, and the structure-to-soil relative inertia, δ for different concrete building classes, i.e., for a different number of stories and resisting systems.

The δ values reported in Table 2 are retrieved, considering a soil mass density ρ equal to 1.8 Mg/m^3; whereas all the structural masses refer to the pure bare frame, the values reported in Table are considered a lower boundary for the final δ selection. According to Table 2, the H/B and δ ratios are investigated in the range (1,2,3,4) and (0.05,0.1,0.2) respectively.

3.1.4 Structure modeling

As shown in Figure 3 for this application, three building classes of low, mid, and high-rise regularly infilled structures designed with low-code prescriptions are selected

Table 2. Literature studies on SSI and site-effects available for Thessaloniki, Greece and main interaction parameters taken as reference

	Mass(Mg)	Stor.	Res. system	2B(m)	H(m)	H/B	δ
Karapetrou et al 2015	207.0	H3	CR-LFM	16.47	10.98	1.3	0.05
Karapetrou et al 2015	207.0	H3	CR-LFM	16.47	10.98	1.3	0.05
Karapetrou et al 2015	334.0	H9	CR-LFM	16	28.5	3.6	0.03
Fotopoulou et al 2012	37.2	H2	CR-LFM	5	7	2.8	0.15
Fotopoulou et al 2012	290.3	H4	CR-LFM	15	12	1.6	0.08
Karafagka et al 2021	65.7	H2	CR-LFM	16	7.5	0.9	0.02
Petridis and Pitilakis 2020	46.4	H2	CR-LDUAL	16	7.5	0.9	0.02
Petridis and Pitilakis 2020	93.5	H4	CR-LDUAL	16	13.5	1.7	0.02
Petridis and Pitilakis 2020	255.7	H9	CR-LDUAL	16	28.5	3.6	0.02
Petridis and Pitilakis 2020	81.7	H2	CR-LFM	16	7.5	0.9	0.03
Petridis and Pitilakis 2020	167.8	H4	CR-LFM	16	13.5	1.7	0.03
Petridis and Pitilakis 2020	403.8	H9	CR-LFM	16	28.5	3.6	0.04

from the Thessaloniki exposure. These are namely the CR-LFINF-DUL-H2, -H4, and -H6, following the GEM taxonomy (D'Ayala et al, 2014). This selection arises out of a need to represent more than 40 percent of the total exposure of Thessaloniki to gain further insights into the urban structural fragility that constitute a prerequisite in the risk calculation. Figure 3 reports the spatial distribution of the chosen structural typologies and their concentration in the urban environment. The ESDoF system representing the selected building classes is characterized by the corresponding elastic perfectly plastic (EPP) backbone curves and by a uniaxial bilinear hysteretic material object with pinching of force and deformation, damage due to ductility and energy, and degraded unloading stiffness based on ductility, as available in OpenSees.

3.2 Analysis

Fragility curves are calculated in this study, estimating damage distributions through nonlinear dynamic cloud analyses of the structural models discussed in section 3.1.4 endowed with the BNWF (section 3.1.3) subjected to seismic loading. The seismic action is estimated by propagating the selected input motions (section 3.1.1) recorded on outcropping rock upward the free surface through one dimensional ($1D$) numerical simulations of seismic site response analysis for all the seven profiles listed in Table 1 and characterized in section 3.1.2.

To provide an overview of the modification of the input motion due to local geotechnical conditions, Figure 4 compares the bedrock and the free-field motions resulting from the performed analyses in terms of acceleration displacement response spectra ($ADRS$). Only two different soil deposits are shown for brevity, corresponding to soil classes C and D, respectively. Overall, site amplification effects are clearly recognizable from the difference between the mean values (thick red and black lines) for all the reference profiles considered in this study. In detail, the maximum amplification for the soft soil profile (Figure 4b) occurs for periods lower than 0.6 s (also evident in other studies on the topic, e.g., de Silva 2020). In comparison, the trend is

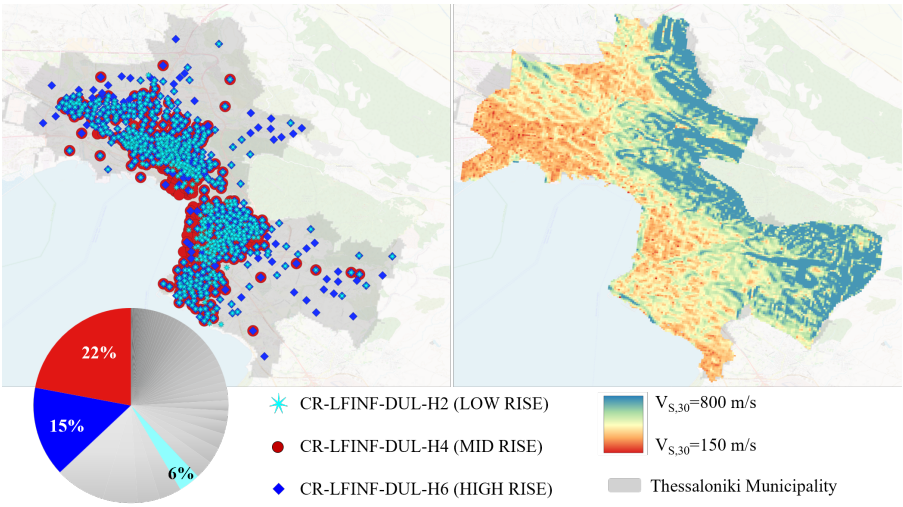

Fig. 3. Distribution of the building classes in Thessaloniki selected for the analysis along with the $V_{S,30}$ map for the Thessaloniki municipality computed following the slope-based approach proposed by Wald and Allen (2007).

inverted for very soft profiles (i.e., class D and Figure 4a) where the seismic demand is maximized for larger periods and is expected to influence more high-rise buildings. The maximum amplification occurs when the soil attains its fundamental frequency, which can be assumed accordingly to the homogeneous soil approximation, around 0.4 s and 0.8 s for the ground classified as Class C and D, respectively, in the provided example.

By processing the results of the cloud analysis, it is possible to correlate the structural response variable and the seismic intensity measurement for all the limit states of interest. The engineering demand parameter (EDP) is assumed to be the critical demand-to-capacity ratio, DCR_{LS} (Jalayer et al 2007), i.e., the ratio between the structural response measure and the structural capacity for the performance of interest, which is equal to unity at the onset of failure (also known as the limit state).

Following previous works (Martins and Silva, 2020), the slight limit state (SD) is assumed to be a fraction of the yield displacement ($0.75Sd_y$). Moderate (MD) and extensive damage (ED) are assumed within a range defined from yield and ultimate displacement, equal to $0.5Sd_y$ +$0.33Sd_u$ and to $0.25Sd_y$ +$0.67Sd_u$ respectively. Finally, complete damage (CD) is considered to be reached at the onset of the ultimate displacement capacity of the structure.

Figure 5 compares the performance of the fixed-base building resting on rock (grey data) with different SSI interacting systems (blue data) for two other soil profiles, corresponding to soil class D (Figure 5a) and B (Figure 5b), respectively. To improve the visual comparison, together with the cloud regressions is also reported the vertical line $DCR_{LS} = 1$, corresponding to the attainment of the slight limit state (SD) and the so-called collapse cases (red data), i.e., the cases leading to structural

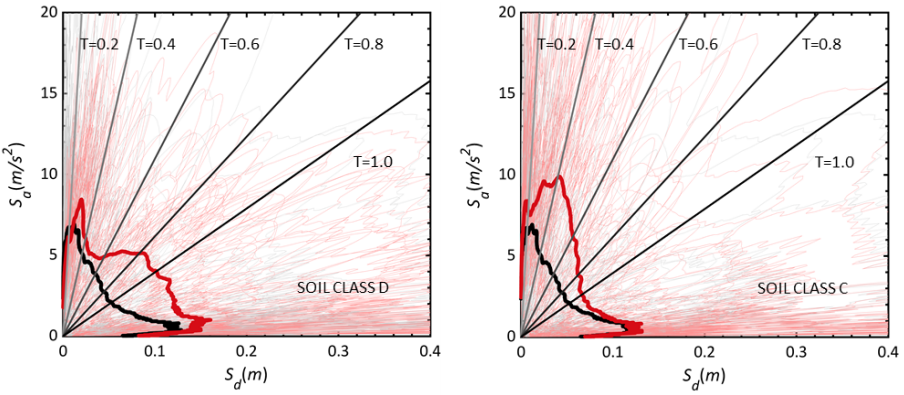

Fig. 4. Pseudo-acceleration-displacement response spectra for all the selected input records (thin black lines) and the corresponding free-field motion as resulting from the site response analysis (thin red lines) along with mean values (thick lines) for two soft soil profiles corresponding to (a) $V_{S,30}$ = 150 and (b) $V_{S,30}$ = 300 m/s.

collapse and/or reaching dynamic instability due to large deformations (Shome and Cornell, 2000). The comparison is made considering the same intensity measure, i.e. spectral acceleration of the outcrop bedrock input motions. Local SA and SSI effects appear evident after a visual comparison among the data trends reported in the plot of Figure 5a where the SSI + SA system generally exhibits a more significant displacement for the same level of intensity measure. As expected, the data points associated with the soil profile representative of soil type B almost overlap with the reference fixed-base data, thus confirming the desired negligible effects of very stiff soil on the seismic response of structures.

Moreover, in all cases where SSI becomes essential, i.e., generally for very soft deposits, large slenderness, and inertia ratios (as in the case of Figure 5a), the collapse cases tend to increase when nonlinear foundation behavior is allowed (red rhombus data) compared to the fixed-base assumption (red circles). Thus, although the flexural displacement, responsible for the damage to the structures, generally tends to decrease when considering only SSI effects, the total displacement demand always increases. Consequently, even only SSI effects may lead to an increase in structural fragility for excessive displacement demand leading to structural instability.

The Modified Cloud analysis (MCA, Jalayer et al (2017)) is used herein to compute fragility functions which formally considers the collapse-inducing records. Collapse cases are defined in literature as the input motions causing structural collapse and/or reaching dynamic instability due to large deformations). In this revised model, the collapse and non-collapse parts are mixed using the 'Total Probability Theorem' as follows:

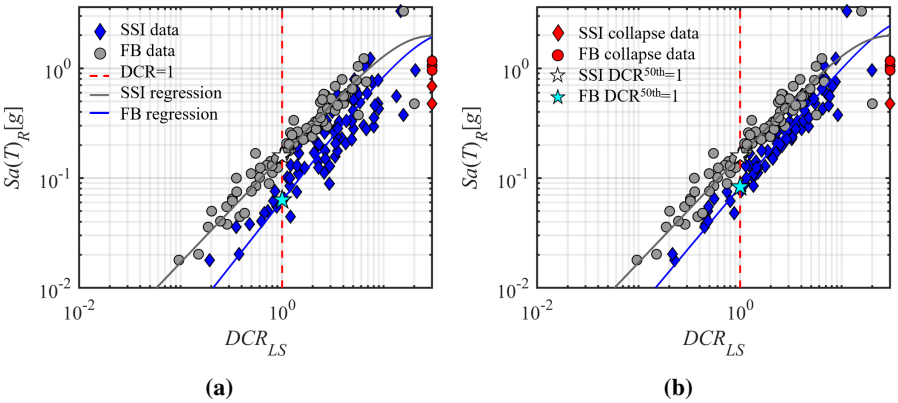

Fig. 5. Cloud analysis results for the slight damage state (SD) for different building–foundation-soil combinations, i.e. for a profile with (a) $V_{S,30}$ = 150 m/s and (b) $V_{S,30}$ = 300 m/s; the vertical dashed red line indicates the attainment of the performance level (limit state function $DCR_{LS} = 1$).

$$P\left(DCR_{LS} > 1|IM\right) = P\left(DCR_{LS} > 1|IM, NoC\right) \cdot \left(1 - P(C|IM)\right) + P\left(DCR_{LS} > 1|IM, C\right) \cdot P(C|IM) \quad (2)$$

The probability of exceeding the performance level for the non-inducing collapse records (grey and blue data depicted in Figure 5) can be computed using the classical cloud approach. The collapse-inducing records (red data) are treated separately. In detail, $P(C|IM)$ is the probability of having collapsed. From Eq. ,2 it is relatively straightforward that as the number of records leading to collapse increases, the resulting structural fragility also increases. Although inherently different, the final regression is expected to diverge from the classical linear one when collapse cases occur, i.e., generally for larger IM values. This method is particularly effective in characterizing the fragility of compliant base structures, which are likely to happen when SSI effects are significant. As the intensity measures reach higher levels, loss of numerical convergence occurs. When the compliance of the foundation soil is also taken into account, dynamic instability in the analysis may occur due to excessive settlements or rocking of the basement without significant damage to the superstructure.

From Figure 5, it can be seen that for the exact value of IM, some records collapse when considering the interaction with the foundation subsoil. In contrast, they do not collapse when following the fixed-base assumption. It is well known in the literature (Gajan et al, 2010) that significant rotation of the foundation is more likely to occur for structures with high aspect ratios. As the soil becomes softer, this kinematic mechanism tends to enhance, being the impedance functions and the foundation stiffness directly proportional to the soil shear modulus. Therefore, this failure mechanism, and consequently collapse cases, are more expected in the case of high values of H/B and low values of $V_{S,30}$.

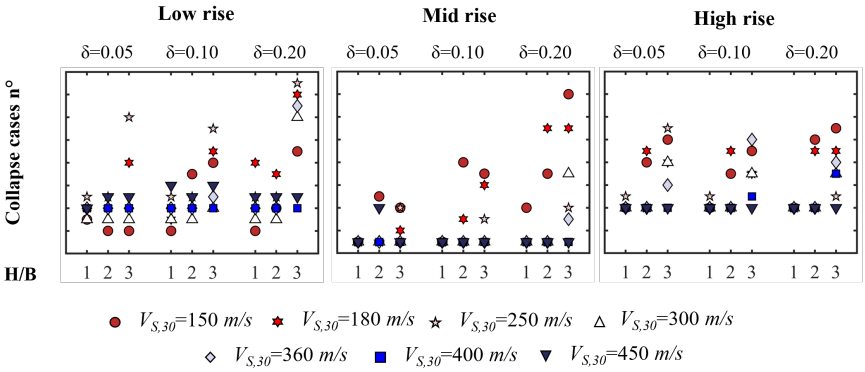

Fig. 6. Collapse cases recorded during the dynamic analyses of the low, medium, and high rise building class (CR-LFINF-DUL) identified by different soil-foundation systems, $H/B = 1, 2, 3, 4$ and $\delta = 0.05, 0.1, 0.2$

In Figure 6, the cases of collapse recorded during the dynamic analyses of the low, medium, and high rise reinforced concrete structures considering the foundation systems discussed in subsection 3.1.3 characterized by different H/B and δ ratios are shown. For comparison, the collapse cases for all seven virtual profiles listed in Table are reported1, from very soft (red data) to stiff (blue points). As expected, for all the building classes under consideration, as the interaction factors H/B and δ increase and the $V_{S,30}$ decreases, the cases of collapse increase. In particular, the cases of collapse for the mid-rise system resting on soil class D (blue data point) identified by a foundation system $H/B = 1$ and $\delta = 0.05$ are null. In contrast, for $H/B = 3$ and $\delta = 0.2$, the cases go up to 14, confirming what stayed before.

To conclude, even though it is common in design and assessment practice to neglect SSI because of the expected beneficial play on the structural safety (mainly due to the predicted demand reduction coming with the inertial effects), in some cases, mostly when SSI effects are essential (high H/B and δ and low $V_{S,30}$), the explicit consideration of nonlinear foundation compliance and consequent collapse cases, leads to an increase of the overall structural fragility.

Finally, the uncertainty of the fragility parameters is estimated through the standard deviation, β_{TOT} which is modeled by the combination of the different variability sources the uncertainty in the damage states, and the record-to-record variability implicitly considered by the randomness of ground motions.

3.3 Output

The results of our methodology are fragility functions considering different SSI and SA scenarios.

Figure 7 reports the comparison of fragility functions developed for a low, mid, and high-rise regularly infilled structure designed with low-code prescriptions (namely CR-LFINF-DUL-H2, -H4, and -H6) by changing the H/B and δ ratio and the $V_{S,30}$ for all the predefined limit states. The fragility functions shown in Figure 7 were

estimated as a function of spectral acceleration at the conditioning period varying for each configuration (i.e., $Sa(T = 0.3s)$ for CR-LFINF-DUL-H2 and $Sa(T = 0.6s)$ for CR-LFINF-DUL-H4, -H6). All in all (see, for example, Figure 7a), the result of the analyses for the flexible foundations, considering SSI and SA effects (dashed lines), produce a shift to the left of the fragility curves compared to the fixed-base case (continuous lines), thus resulting into an increase of the structural fragility.

The fragility shift is more pronounced for very soft soil profiles. See for example Figure 7c developed for the virtual soil profile corresponding to $V_{S,30}$ 180 m/s compared to Figure 7d for $V_{S,30}$ 360 m/s. Indeed, for mid- and high-rise structures, i.e., for flexible systems characterized by a long fundamental period of T>0.6s, the spectral acceleration is generally expected to reduce for medium-soft profiles (Figure ,4b) leading to an increase just in the case of Class D soil profiles (see Figure 4a).

On the other hand, SSI may play a significant role in increasing the seismic base shear force for the low-rise structure. Generally, the fixed-base period of low-rise buildings being minimal may lie within the initial sharply-increasing zone of the response spectrum (red curve in Figure 4). Hence, in such cases, site amplification effects may play an important role, but also, period elongation associated with SSI may cause an increase in the spectral acceleration ordinate. This results in an overall increase in the structural fragility, as shown in Figure 7c, 7d.

When comparing the fragility functions developed for the selected building classes resting on the same soft soil profiles. Still, by accounting for different hypotheses on the BNWF systems by varying the H/B and δ ratio, it is possible to appreciate the variability associated with the SSI phenomenon in the fragility computation (see Figure 8), especially when SSI is expected to be significant, (i.e., again for large values of H/B and δ ratios).

The scatter between the results is likely to be more pronounced for high damage states due to the nonlinear soil-foundation phenomenon occurring under strong events, i.e., large IM values. The uncertainty in the definition of the soil-foundation configuration cannot be neglected for the complete damage state (red curves in Figure 8) even for the medium soft profile characterized by $V_{S,30}$ = 360m/s.

Considering the number of records, intensity levels, and a possible parameterization of the structural characteristics, several thousands of time-history analyses are typically carried out in such studies. The seismic fragility curves, including SA and SSI effects, show up to now, where the given intensity measure refers to the analysis input records (i.e., as recorded on rock/stiff soil) and can be used when the hazard scenario is referring to the underlying bedrock or generally adopted to gain insights into the differences concerning the typical assessment practice which considers fixed-base structures and neglects the modification of the input motion due to the deformability of the soil profile (as in the case of Figure 7a). On the other hand, the fragility curves as a function of intensity measures defined from the free-field motions can also be used in the framework of a risk assessment where the hazard includes site-effects adopting either code- or research-based amplification factors or moreover where the hazard scenario comes directly from physics-based numerical simulations.

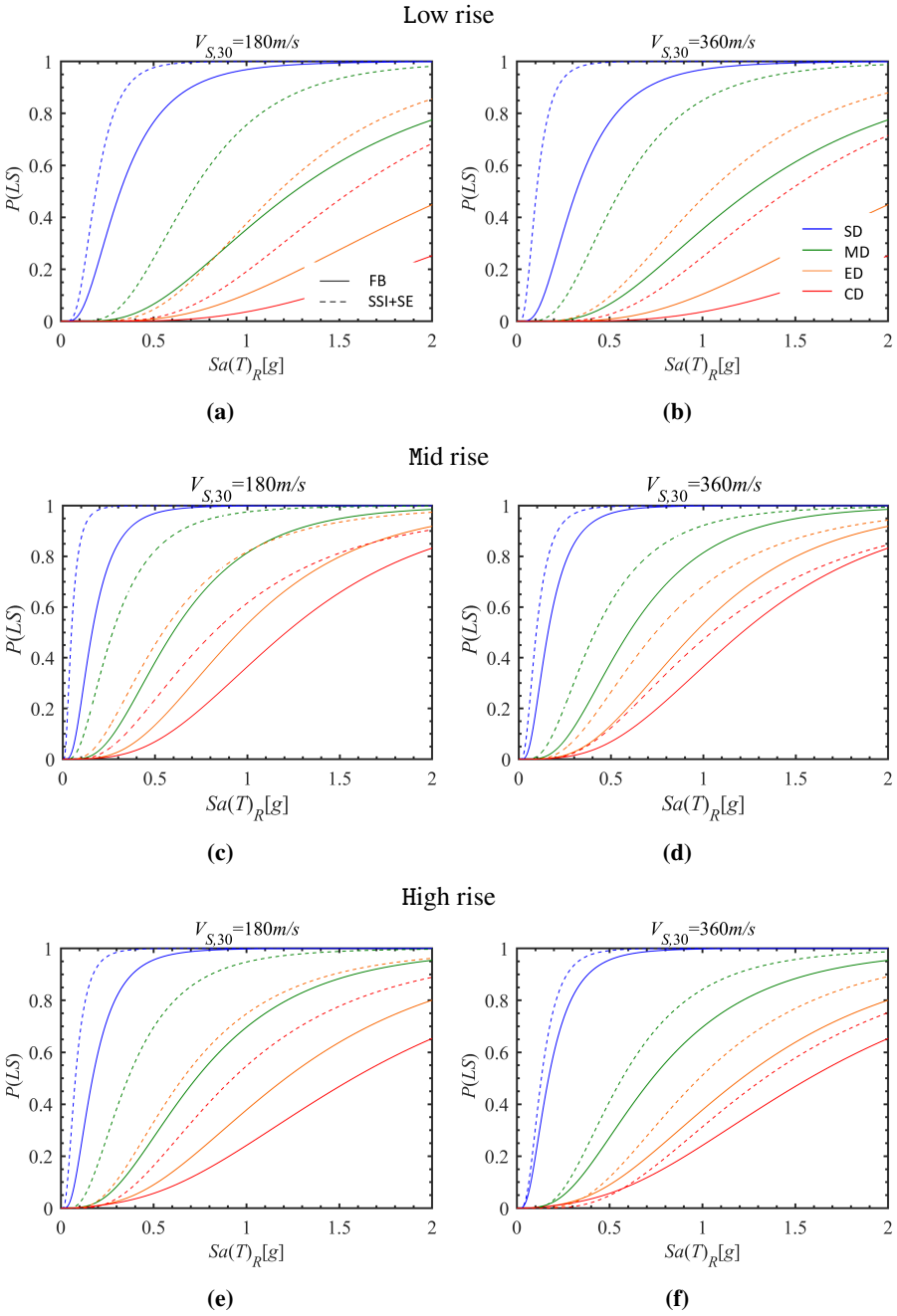

Fig. 7. Comparison between fragility functions in terms of $Sa(T)_R$ developed for the selected building classes, i.e. CR-LFINF-DUL low (a,b), mid (c,d) and high rise (e,f) considering the structure fixed at its base (continuous lines) and SSI and site-effects for one BNWF system characterized by $H/B = 1$, $\delta = 0.05$ and (a,c,e) $V_{S,30}$ = 180m/s and (b,d,f) $V_{S,30}$ = 360m/s (dashed lines).

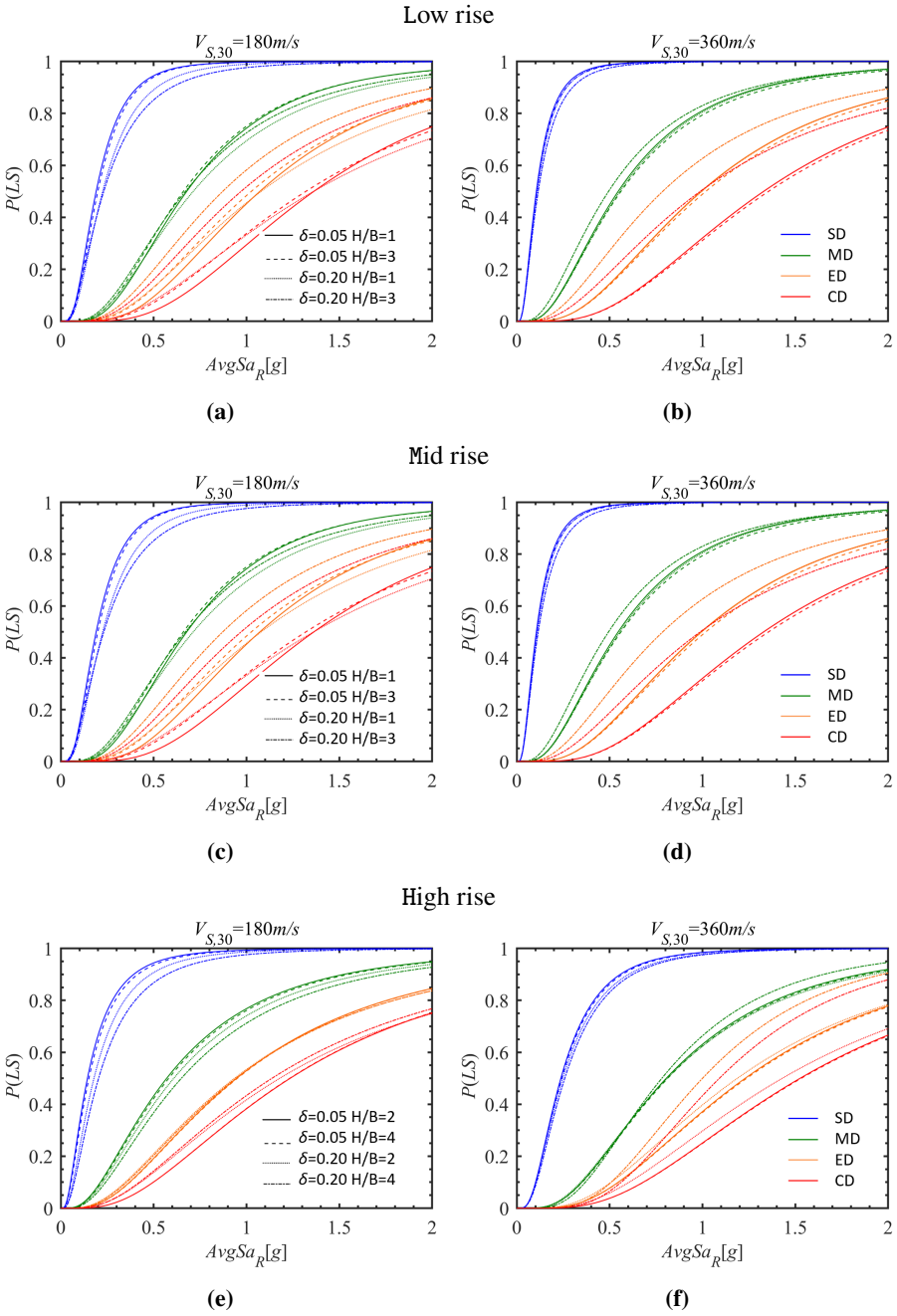

Fig. 8. Fragility functions in terms of $AvgSa_R$ developed for the selected building classes, i.e. CR-LFINF-DUL low (a,b), mid (c,d) and high rise (e,f) considering SSI and site-effects accounting for different hypotheses on the BNWF system, i.e. by low H/B and low δ ratios (continuous lines),high H/B and low δ ratios (dashed lines), low H/B and high δ = 0.2 ratios (dotted lines) and high H/B and high δ = 0.2 ratios (dashed-dot lines) for (a,c,e) very soft soil profile characterized by $V_{S,30}$ = 180m/s and (b,d,f) soft profile characterized by $V_{S,30}$ = 360m/s.

3.4 Risk model

The final goal of this work is to provide the reader with proof on the applicability of the proposed approach in the framework of an urban-scale risk assessment. The fragility functions accounting for different hypotheses on the soil-foundation configuration are integrated with the seismic hazard of Thessaloniki. The main results lead to understanding the role of SSI and SA in the final risk calculation, rather than being limited to the structural fragility assessment.

Following the performance-based earthquake engineering (PBEE) framework, (Cornell and Krawinkler, 2001) the fragility curves shown in subsection 3.3 are adopted to estimate the nominal probability of failure of the different building classes outlined in section 3.1.4 supposed to be located in sites with other geotechnical conditions. The likelihood of failure can be quantified as the expected number in one year of earthquakes capable of causing the exceedance of a predefined performance level, also known as failure rate, λ_F as follows:

$$\lambda_F = \int P\left(DCR_{LS} > 1 | IM\right) \cdot d\lambda_x \ . \tag{3}$$

where the first part of the integral represents the structural fragility and $d\lambda_x$ the absolute value of the differential of the hazard curve. The hazard is computed using the Openquake platform (Pagani et al, 2014) for a reduced number probability of exceedance (POE) and then interpolated to reduce the computational burden. The open-access uniform European seismic risk model, ESRM20 (Crowley et al, 2021) recently developed in the Horizon 2020 EU SERA project framework (SER, SERA) is adopted. Consistent with the proposed approach, the hazard is computed at the outcropping bedrock and is estimated in terms of spectral acceleration, Sa, at two oscillator periods, T=0.3s and T=0.6s for a reference site within the Thessaloniki municipality.

The so-calculated seismic hazard is integrated with the probabilistic representation of seismic fragility for the selected building classes to evaluate the failure rate. Figure 9 presents the computed rates with different colors and markers corresponding to different soil-foundation typologies and configurations (i.e., different $V_{S,30}$, H/B and δ ratio), with respect to the complete damage performance level.

From Figure 9 appears that all the considerations made on SSI and SA effects on fragility functions are similarly reflected in λ_F. Failure rates are generally more significant when considering SSI and SA effects with respect to the reference fixed-base case neglecting SSI and SA (black line in Figure 9). Such an increase is again more pronounced for the very soft soil profiles (data corresponding to $V_{S,30}$=150 or 180m/s) and for large values of δ and H/B ratio. The blue, yellow, and grey data, which correspond to δ equal to 0.2 and H/B equal to 2, 3, and 4, respectively, are always in the uppermost part of the graph. When the soil becomes stiffer, all the soil-foundation configurations show similar results, with a consequent overlap of the data points in Figure 9.

From a visual comparison of Figure 9, for the fixed-base reference case (black horizontal line), the failure rates increase as the structure's height becomes more significant, i.e., from low to high rise. On the contrary, when considering the compliance

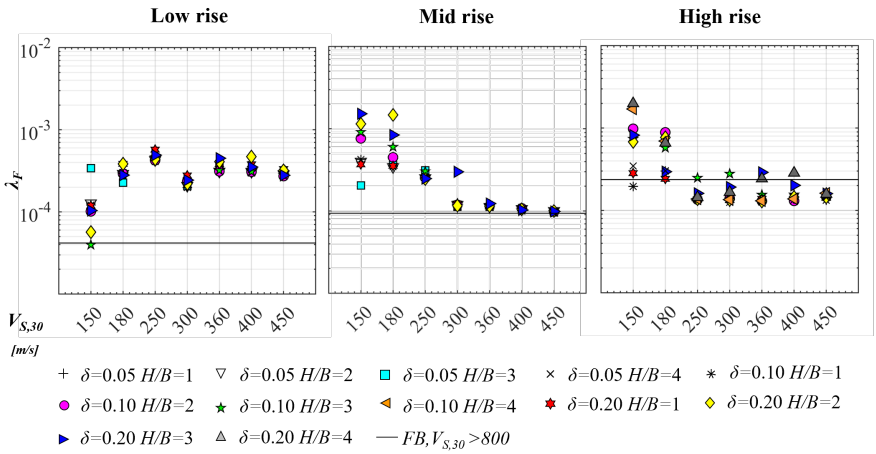

Fig. 9. Comparisons of failure rates for the low, mid, and high rise building class site computed with fragilities from different SSI scenarios

of the foundation soil, this tendency is almost inverted. For the low-rise case where SSI has been shown in the previous sections to play a crucial role, failure rates, especially in the soft-medium soil profile range, are higher than in mid- and high-rise buildings. For the latter case, the flexibility of the base may also lead to a decrease in the risk compared to the fixed-base case. It is worth remembering that the hazard is convoluted in the range of intensity measures where the fragility calculated considering SSI and site amplification effects, due to the more larger uncertainties, becomes lower than the fixed-base case.

The failure rates of the analyzed building class for all the soil classes are also summarized in Table 3. Even from Table 3 can be pointed out that although the estimated fragility parameters show a substantial dependency on the soil-foundation system, it can be observed that the resulting failure rates, thanks to the filtering effect of low exceedance rates of the most significant IM values (Suzuki and Iervolino, 2019), are relatively close between each other except for the very soft soil profile corresponding to $V_{S,30}$=150 m/s, where again the variability was already observed in the fragility curves.

To conclude, the difference in failure rates indicates that the standard way of fragility calculation, especially for a structure interacting with soft soil profiles, may lead to different results in the final risk calculation.

4 Conclusions

We propose a comprehensive novel framework for the fragility assessment of structures considering the influence of SSI and local site amplification effects, suitable for large-scale applications. One of the greatest uncertainties in studying the problem of SSI is the definition of the main features defining the interactive system. With this in

Table 3. Failure rates corresponding to CD state calculated convoluting the hazard for Thessaloniki and the fragilities of the low, mid and high rise selected building class site (i.e. CR-LFINF-DUL) accounting for multiple SSI+site-effects scenarios

$V_{S,30}[m/s]$	150	180	250	300	360	400	450	>800	
δ=0.05 H/B=1	1.0E-04	2.7E-04	4.1E-04	2.3E-04	3.2E-04	3.1E-04	2.7E-04		
δ=0.05 H/B=2	1.3E-04	2.9E-04	4.3E-04	2.1E-04	3.1E-04	3.1E-04	2.9E-04		
δ=0.05 H/B=3	3.4E-04	2.3E-04	4.4E-04	2.1E-04	3.5E-04	3.1E-04	2.9E-04		
δ=0.10 H/B=1	1.2E-04	3.0E-04	4.1E-04	2.0E-04	3.3E-04	3.0E-04	2.7E-04		
δ=0.10 H/B=2	1.0E-04	2.9E-04	4.3E-04	2.4E-04	3.1E-04	3.1E-04	2.7E-04	3.3E-05	Low rise
δ=0.10 H/B=3	4.0E-05	2.9E-04	4.6E-04	2.2E-04	3.2E-04	3.1E-04	2.8E-04		
δ=0.20 H/B=1	1.2E-04	3.8E-04	5.7E-04	2.8E-04	3.8E-04	3.8E-04	3.3E-04		
δ=0.20 H/B=2	5.7E-05	3.8E-04	4.4E-04	2.2E-04	4.1E-04	4.7E-04	3.2E-04		
δ=0.20 H/B=3	1.0E-04	2.8E-04	4.9E-04	2.4E-04	4.5E-04	3.5E-04	2.8E-04		
δ=0.05 H/B=1	4.2E-04	3.6E-04	2.6E-04	1.2E-04	1.2E-04	1.1E-04	9.8E-05		
δ=0.05 H/B=2	4.0E-04	3.4E-04	2.5E-04	1.2E-04	1.1E-04	1.1E-04	1.0E-04		
δ=0.05 H/B=3	2.0E-04	4.0E-04	3.1E-04	1.1E-04	1.1E-04	1.1E-04	9.7E-05		
δ=0.10 H/B=1	4.2E-04	3.5E-04	2.6E-04	1.2E-04	1.2E-04	1.1E-04	1.0E-04		
δ=0.10 H/B=2	7.6E-04	4.5E-04	2.5E-04	1.2E-04	1.2E-04	1.1E-04	9.8E-05	8.2E-05	Mid rise
δ=0.10 H/B=3	9.1E-04	6.0E-04	3.0E-04	1.2E-04	1.1E-04	1.0E-04	9.7E-05		
δ=0.20 H/B=1	3.7E-04	3.5E-04	2.6E-04	1.2E-04	1.1E-04	1.1E-04	1.0E-04		
δ=0.20 H/B=2	1.1E-03	1.5E-03	2.4E-04	1.2E-04	1.1E-04	1.0E-04	1.0E-04		
δ=0.20 H/B=3	1.5E-03	8.4E-04	2.5E-04	3.0E-04	1.2E-04	1.0E-04	9.9E-05		
δ=0.05 H/B=2	2.0E-04	3.0E-04	1.4E-04	1.3E-04	1.3E-04	1.3E-04	1.3E-04		
δ=0.05 H/B=3	9.8E-04	8.9E-04	1.4E-04	1.4E-04	1.3E-04	1.3E-04	1.5E-04		
δ=0.05 H/B=4	7.4E-04	5.8E-04	2.5E-04	2.8E-04	1.5E-04	1.6E-04	1.6E-04		
δ=0.10 H/B=2	2.8E-04	2.4E-04	1.4E-04	1.3E-04	1.4E-04	1.5E-04	1.4E-04		
δ=0.10 H/B=3	6.8E-04	7.7E-04	1.4E-04	1.3E-04	1.3E-04	1.5E-04	1.4E-04	2.1E-04	High rise
δ=0.10 H/B=4	8.2E-04	3.0E-04	1.6E-04	1.9E-04	2.9E-04	2.0E-04	1.6E-04		
δ=0.20 H/B=2	3.5E-04	3.0E-04	1.4E-04	1.3E-04	1.3E-04	1.3E-04	1.4E-04		
δ=0.20 H/B=3	1.7E-03	7.0E-04	1.4E-04	1.4E-04	1.3E-04	1.4E-04	1.6E-04		
δ=0.20 H/B=4	2.0E-03	6.6E-04	1.4E-04	1.7E-04	2.4E-04	2.8E-04	1.6E-04		

mind, the applicability of the proposed approach relies upon globally available data regarding the soil parameters, the foundation, and the building taxonomy.

To prove the feasibility of the proposed framework, the risk assessment for the most commonly met buildings of Thessaloniki's exposure is computed, in terms of annual failure rates, following the performance-based earthquake engineering framework.

The extensive examination of fragility curves and failure rates demonstrate that SSI and local SA effects are generally more pronounced in the case of soft soil formations and low-rise structures, causing considerable modification to the resulting fragility functions compared to the fixed-base assumption. Moreover, the uncertainties associated with the definition of the soil-foundation system can further affect the results. Neglecting all these effects may lead to underestimating the seismic risk. Therefore, this study encourages the adoption of SSI and site amplification models in the fragility computation, contrary to more simplified approaches for large-scale applications, to promote a more accurate quantification of the potential fragility or failure estimates.

Acknowledgments. The Authors would like to thank Filomena de Silva, Christos Petridis and Evi Riga for the fruitful discussions during the course of this research.

Statements & Declarations. The Authors have received funding from the ITN-Marie Sklodowska-Curie project "New challenges for Urban Engineering Seismology (URBASIS-EU)" (GA 813137).

The authors have no relevant financial or non-financial interests to disclose.

References

(ISESD) . http://www.isesd.hi.is/

(ITACA) . http://itaca.mi.ingv.it

(NGAWEST) . https://ngawest2.berkeley.edu/

(ONEGEO) . http://portal.onegeology.org/

(SERA) . http://www.sera-eu.org/en/home/

(USGS) . https://www.usgs.gov/programs/earthquake-hazards/science/vs30-models-and-data

Amendola C, Pitilakis D (2022) Vulnerability assessment of historical cities including ssi and site-effects. In: TC 301 - IS NAPOLI 2022, Third international symposium on Geotechnical Engineering For The Preservation Of Monuments And Historic Sites Napoli, Italy, 22–24 June 2022, June, pp 22–24

Amendola C, Silva FD, Pitilakis D, et al (2021) On the effectiveness of experimentally-derived foundation impedance functions. In: COMPDYN 2021 8th ECCOMAS Thematic Conference on Computational Methods in Structural Dynamics and Earthquake Engineering M. Papadrakakis, M. Fragiadakis (eds.) Streamed from Athens, Greece, 27–30 June 2021, June, pp 27–30

Bazzurro P, Cornell CA (2004) Ground-motion amplification in nonlinear soil sites with uncertain properties. Bulletin of the Seismological Society of America 94(6):2090–2109. https://doi.org/10.1785/0120030215

Brunelli A, de Silva F, Cattari S (2022) Site effects and soil-foundation-structure interaction: derivation of fragility curves and comparison with codes-conforming approaches for a masonry school. Soil Dynamics and Earthquake Engineering 154(June 2021):107,125. https://doi.org/10.1016/j.soildyn.2021.107125

Brzev S, Scawthorn C, Charleson AW, et al (2013) Gem building taxonomy (version 2.0). Tech. rep., GEM Foundation

Cavalieri AAF. & Correia, Crowley H, Pinho R (2020) Dynamic soil-structure interaction models for fragility characterisation of buildings with shallow foundations. Soil Dynamics and Earthquake Engineering 132:106,004. https://doi.org/10.1016/j.soildyn.2019.106004

CEN (2005) Eurocode 8: Design of structures for earthquake resistance-part 1: general rules, seismic actions and rules for buildings. European Standard EN 1998-1:2004 Brussels, Belgium: European Committee for Standardisation

Cornell CA, Krawinkler H (2001) A framework for performance-based seismic design. Structures 2001: A Structural Engineering Odyssey pp 1–1

Crowley H, Dabbeek J, Despotaki V, et al (2021) European seismic risk model (esrm20), efehr technical report 002, v1.0.0 https://doi.org/https://doi.org/10.7414/EUC-EFEHR-TR002-ESRM20

D'Ayala D, Meslem A, Vamvatsikos D, et al (2014) Guidelines for analytical vulnerability assessment of low/mid-rise buildings, vulnerability global component project. GEM Technical Report 2015-08 v100 08:162

De Risi R, Penna A, Simonelli AL (2019) Seismic risk at urban scale: the role of site response analysis. Soil Dynamics and Earthquake Engineering 123(February):320–336. https://doi.org/10.1016/j.soildyn.2019.04.011

Derras B, Bard PY, Cotton F (2017) VS30, slope, H800 and f0: Performance of various site-condition proxies in reducing ground-motion aleatory variability and predicting nonlinear site response 4. Seismology. Earth, Planets and Space 69(1). https://doi.org/10.1186/s40623-017-0718-z

Figini R, Paolucci R, Chatzigogos C (2012) A macro-element model for non-linear soil–shallow foundation–structure interaction under seismic loads: theoretical development and experimental validation on large scale tests. Earthquake Engineering & Structural Dynamics 41(3):475–493

Forte G, Fabbrocino S, Fabbrocino G, et al (2017) A geolithological approach to seismic site classification: an application to the molise region (italy). Bulletin of Earthquake Engineering 15(1):175–198. https://doi.org/10.1007/s10518-016-9960-1

Fotopoulou S, Karapetrou S, Pitilakis K (2012) Seismic vulnerability of rc buildings considering ssi and aging effects. 15th World Conference on Earthquake Engineering

Gajan S, Raychowdhury P, Hutchinson TC, et al (2010) Application and Validation of Practical Tools for Nonlinear Soil-Foundation Interaction Analysis. Earthquake Spectra 26(1):111–129. https://doi.org/10.1193/1.3263242, URL http://link.aip.org/link/EASPEF/v26/i1/p111/s1{&}Agg=doihttp://journals.sagepub.com/doi/10.1193/1.3263242

Harden C, Hutchinson T, Martin GR (2005) Numerical Modeling of the Nonlinear Cyclic Response of Shallow Foundations. Pacific earthquake engineering research center

Jalayer F, F. P, Pinto PE (2007) A scalar damage measure for seismic reliability analysis of rc frames. Earthquake Engineering and Structural Dynamics 36(June):2059–2079. https://doi.org/10.1002/eqe

Jalayer HF.and Ebrahimian, Miano A, Manfredi G, et al (2017) Analytical fragility assessment using unscaled ground motion records. Earthquake Engineering and Structural Dynamics 46(15):2639–2663. https://doi.org/10.1002/eqe.2922

Karafagka S, Fotopoulou S, Pitilakis D (2021) Fragility curves of non-ductile rc frame buildings on saturated soils including liquefaction effects and soil–structure interaction. Bulletin of Earthquake Engineering 19(15):6443–6468

Karapetrou ST, Fotopoulou SD, Pitilakis KD (2015) Seismic vulnerability assessment of high-rise non-ductile rc buildings considering soil-structure interaction effects. Soil Dynamics and Earthquake Engineering 73:42–57. https://doi.org/10.1016/j.soildyn.2015.02.016

Martins L, Silva V (2020) Development of a fragility and vulnerability model for global seismic risk analyses. Bulletin of Earthquake Engineering https://doi.org/10.1007/s10518-020-00885-1

Mazzoni S, McKenna F, Scott MH, et al (2006) Opensees command language manual. Pacific Earthquake Engineering Research (PEER) Center 264:137–158

NIST G (2012) Soil-structure interaction for building structures. https://doi.org/12-917-21

Pagani M, Monelli D, Weatherill G, et al (2014) Openquake engine: An open hazard (and risk) software for the global earthquake model. Seismological Research Letters 85(3):692–702

Petridis C, Pitilakis D (2020) Fragility curve modifiers for reinforced concrete dual buildings, including nonlinear site effects and soil–structure interaction. Earthquake Spectra https://doi.org/10.1177/8755293020919430

Petridis C, Pitilakis D (2021) Large-scale seismic risk assessment integrating nonlinear soil behavior and soil–structure interaction effects. Bulletin of Earthquake Engineering https://doi.org/10.1007/s10518-021-01237-3

Pitilakis D, Petridis C (2020) Fragility curves for existing reinforced concrete buildings, including soil-structure interaction and site amplification effects,. Submitted to Engineering Structures

Pitilakis K, Karapetrou ST, Fotopoulou SD (2014) Consideration of aging and ssi effects on seismic vulnerability assessment of rc buildings. Bulletin of Earthquake Engineering 12:1755–1776. https://doi.org/10.1007/s10518-013-9575-8

Pitilakis K, Riga E, Anastasiadis A, et al (2019) Towards the revision of ec8: Proposal for an alternative site classification scheme and associated intensity dependent spectral amplification factors. Soil Dynamics and Earthquake Engineering 126:105,137. https://doi.org/10.1016/j.soildyn.2018.03.030

Rajeev P, Tesfamariam S (2012) Seismic fragilities of non-ductile reinforced concrete frames with consideration of soil structure interaction. Soil Dynamics and Earthquake Engineering 40:78–86. https://doi.org/10.1016/j.soildyn.2012.04.008

Raychowdhury P, Hutchinson TC (2008) Shallowfoundationgen opensees documentation. Open System for Earthquake Engineering Simulation (OpenSEES): University of California, San Diego

Riga E, Karatzetzou A, Mara A, et al (2017) Studying the uncertainties in the seismic risk assessment at urban scale applying the capacity spectrum method: The case of thessaloniki. Soil Dynamics and Earthquake Engineering 92:9–24. https://doi.org/https://doi.org/10.1016/j.soildyn.2016.09.043, URL https://www.sciencedirect.com/science/article/pii/S0267726116303220

Riga E, Karatzetzou A, Apostolaki S, et al (2021) Verification of seismic risk models using observed damages from past earthquake events. Bulletin of Earthquake Engineering 19(2):713–744

Saez E, Lopez-Caballero F, Modaressi-Farahmand-Razavi A (2011) Effect of the inelastic dynamic soil–structure interaction on the seismic vulnerability assessment. Structural safety 33(1):51–63

Shome N, Cornell CA (2000) Structural seismic demand analysis: consideration of collapse. In: 8th ASCE Specialty Conference on Probabilistic Mechanics and Structural Reliability, pp 1–6

de Silva F (2020) Influence of soil-structure interaction on the site-specific seismic demand to masonry towers. Soil Dynamics and Earthquake Engineering 131:106,023. https://doi.org/10.1016/j.soildyn.2019.106023

Smerzini C, Pitilakis K (2018) Seismic risk assessment at urban scale from 3d physics-based numerical modeling: the case of thessaloniki. Bulletin of Earthquake Engineering 16(7):2609–2631

Stewart JP, Fenves GL, Seed RB (1999) Seismic soil-structure interaction in buildings. i: Analytical methods. Journal of Geotechnical and Geoenvironmental Engineering 125(1):26–37

Stewart JP, Kim S, Bielak J, et al (2003) Revisions to Soil-Structure Interaction Procedures in NEHRP Design Provisions. Earthquake Spectra 19(3):677–696. https://doi.org/10.1193/1.1596213

Suzuki A, Iervolino I (2019) Seismic fragility of code-conforming italian buildings based on sdof approximation. Journal of Earthquake Engineering https://doi.org/10.1080/13632469.2019.1657989

Tomeo R, Pitilakis D, Bilotta A, et al (2018) Ssi effects on seismic demand of reinforced concrete moment resisting frames. Engineering Structures 173:559–572

Tropeano G, Soccodato FM, Silvestri F (2018) Re-evaluation of code-specified stratigraphic amplification factors based on italian experimental records and numerical seismic response analyses. Soil Dynamics and Earthquake Engineering 110(December 2017):262–275. https://doi.org/10.1016/j.soildyn.2017.12.030

Veletsos AS, Meek JW (1974) Dynamic behaviour of building-foundation systems. Earthquake Engineering & Structural Dynamics 3(2):121–138

Vratsikidis A, Pitilakis D (2019) Soil mass participation in soil-structure interaction by field experiments in EuroProteas. In: Silvestri, Moraci (eds) Proceedings of the 7th International Conference on Earthquake Geotechnical Engineering, Rome, Italy, pp 681–688

Wald DJ, Allen TI (2007) Topographic slope as a proxy for seismic site conditions and amplification. Bulletin of the Seismological Society of America 97(5):1379–1395. https://doi.org/10.1785/0120060267

Yepes-Estrada C, Silva V, Rossetto T, et al (2016) The global earthquake model physical vulnerability database. Earthquake Spectra 32(4):2567–2585

Appendix A

Table A1. Suite of strong ground-motion recorded on rock/firm soil selected for performing nonlinear dynamic analysis

n°	EQID	Earthquake Name	Year	Mw	EpiD (km)	$V_{S,30}$ (m/s)	PGA (g)
1	0129	Kobe, Japan	1995	6.90	25.40	1043	0.30
2	0145	Sierra Madre	1991	5.61	39.60	996	0.10
3	0118	Loma Prieta	1989	6.93	20.35	1070	0.44
4	0113	Whittier Narrows-01	1987	5.99	13.85	969	0.10
5	0127	Northridge-01	1994	6.69	18.99	1222	0.14
6	0255	Molise-02, Italy	2002	5.7	58.33	865	0.04
7	0144	Manjil, Iran	1990	7.37	40.43	724	0.52
8	0179	Parkfield-02, CA	2004	6.00	6.82	907	0.20
9	0176	Tottori, Japan	2000	6.61	31.41	967	0.20
10	0137	Chi-Chi, Taiwan	1999	7.62	80.53	1526	0.10
11	0274	L'Aquila, Italy	2009	6.30	1.75	717	0.35
12	0224	Umbria-03, Italy	1984	5.6	17.08	922	0.07
13	0237	Umbria Marche (aftershock 1)	1997	5.5	14.86	694	0.19
14	IT-1998-0103	SOUTHERN_ITALY	1998	5.6	18	1024	0.16
15	IT-1990-0003	SICILY	1990	5.6	36.9	871	0.11
16	IT-2012-0061	COSENZA	2012		2.4	1906	0.18
17	IT-1979-0009	NORCIA	1979	5.8	9.3	698	0.21
18	IT-1984-0004	LAZIO_ABRUZZO	1984	5.9	10.1		0.11
19	EMSC-20161030	CENTRAL_ITALY	2016	6.5	11		0.93
20	EMSC-20181226	SICILY_ITALY	2018	4.9	4.5		0.55
21	IT-2013-0009	NORTHERN_ITALY	2013	4.5	2.1		0.23
22	0279	Iwate	2008	6.90	23.17	826	0.27
23	0180	Niigata, Japan	2004	6.63	58.35	829	0.11
24	55X	Friuli	1976	6.5	23		0.35
25	55Y	Friuli	1976	6.5	23		0.35
26	3	Friuli	1976	6.5	101		0.03
27	4	Friuli (aftershock)	1976	6	12		0.13
28	46	Avej	2002	6.5	28		0.44
29	21	Duzce 1	1999	7.2	34		0.12
30	44	Duzce 1	1999	7.2	23		0.49
31	28	Strofades	1997	6.6	90		0.06
32	27	Strofades	1997	6.6	136		0.07
33	9	Campano Lucano	1980	6.9	23		0.14
34	12	Campano Lucano	1980	6.9	80		0.06
35	11	Campano Lucano	1980	6.9	25		0.06
36	13	Campano Lucano	1980	6.9	127		0.02
37	10	Campano Lucano	1980	6.9	32		0.21
38	14	Biga	1983	6.1	56		0.05
39	45	Bingol	2003	6.3	14		0.51
40	8	Montenegro (aftershock)	1979	6.2	30		0.07
41	7	Montenegro	1979	6.9	65		0.22
42	6	Montenegro	1979	6.9	21		0.18
43	5	Tabas	1978	7.3	12		0.33
44	19	Izmit	1999	7.6	9		0.16
45	20	Izmit	1999	7.6	78		0.05
46	18	Izmit	1999	7.6	47		0.23
47	16	Umbria Marche	1997	6	21		0.18
48	15	Umbria Marche	1997	6	79		0.06
49	17	Umbria Marche	1997	6	25		0.07
50	26	Kalamata	1997	6.4	48		0.12
51	30	Kozani	1995	6.5	17		0.20
52	29	Off coast of Magion Oros	1983	6.6	76		0.11
53	40	South Iceland (aftershock)	2000	6.4	6		0.52
54	41	South Iceland (aftershock)	2000	6.4	15		0.12
55	37	South Iceland (aftershock)	2000	6.4	14		0.18
56	43	South Iceland (aftershock)	2000	6.4	5		0.73
57	23	South Iceland	2000	6.5	13		0.13
58	35	South Iceland	2000	6.5	15		0.35
59	36	South Iceland	2000	6.5	41		0.11
60	22	South Iceland	2000	6.5	5		0.31